Ross Stein

Relationship of Regional and Local Structures to Mount Pinatubo Activity

By Bartolome C. Bautista,[1] Ma. Leonila P. Bautista,[1] Ross S. Stein,[2] Edito S. Barcelona,[1] Raymundo S. Punongbayan,[1] Eduardo P. Laguerta,[1] Ariel R. Rasdas,[1] Gemme Ambubuyog,[1] and Erlinda Q. Amin[1]

in

FIRE and MUD

Eruptions and Lahars of Mount Pinatubo, Philippines

Edited by

CHRISTOPHER G. NEWHALL
Geologist, U.S. Geological Survey
Affiliate Professor, University of Washington Volcano Systems Center

RAYMUNDO S. PUNONGBAYAN
Director, Philippine Institute of Volcanology and Seismology

1996

Philippine Institute of Volcanology and Seismology
Quezon City

University of Washington Press
Seattle and London

Relationship of Regional and Local Structures to Mount Pinatubo Activity

By Bartolome C. Bautista,[1] Ma. Leonila P. Bautista,[1] Ross S. Stein,[2] Edito S. Barcelona,[1] Raymundo S. Punongbayan,[1] Eduardo P. Laguerta,[1] Ariel R. Rasdas,[1] Gemme Ambubuyog,[1] and Erlinda Q. Amin[1]

ABSTRACT

The spatial and temporal proximity of the 1990 M_s 7.8 Luzon earthquake and reawakening of Mount Pinatubo in 1991 hints at the possibility of a relation between the two events. Composite focal-plane solutions for preeruption and posteruption microearthquakes, fault plane solutions for M>5 syneruption events, and information about the local and regional faults suggest that movement along these regional faults preceded, accompanied, and followed the major eruption of Mount Pinatubo in June 1991.

Changes in Coulomb failure stress along faults of the Pinatubo area, as a result of the Luzon earthquake, were on the order of 0.1 bar and probably were not a cause of Pinatubo's reawakening. However, compressive stress on the magma reservoir and its roots was about 1 bar, possibly enough to squeeze a small volume of basalt into the overlying dacitic reservoir. Alternatively, strong ground shaking associated with the Luzon earthquake might have done the same or triggered movement along previously stressed faults that in turn allowed magma ascent.

INTRODUCTION

When Mount Pinatubo reawoke in 1991 from a 500-yr slumber, many scientists asked, "Was the 1991 eruption triggered by, or otherwise related to, the M_s 7.8 Luzon earthquake that had occurred on July 16, 1990?" One way to address this question is through the study of earthquakes that occurred after the July 16, 1990, Luzon earthquake and before, during, and after the big eruption. To test for a relation, we asked:

1. Did aftershocks of the 1990 Luzon earthquake occur at and near Mount Pinatubo?
2. How did seismicity that led to, accompanied, and followed the eruption relate to local and regional faults and to pre-1990 seismicity?
3. Was predicted stress change at Pinatubo from the July 16 earthquake of a sense and magnitude that might have triggered magma ascent?

REGIONAL AND LOCAL STRUCTURES

Mount Pinatubo is a part of the Luzon arc, whose volcanism is related to the activity of the Manila trench, located about 120 km west of the volcano (fig. 1). The trench is a product of the active subduction of the South China Sea Plate beneath Luzon island. Convergence is roughly east-west.

The northwest-trending, left-lateral Philippine fault passes northeast of Mount Pinatubo, and on July, 16, 1990, a 125-km-long segment of this fault ruptured and produced a M_s 7.8 earthquake. The epicenter of this earthquake was about 100 km northeast of Mount Pinatubo.

Closer to Mount Pinatubo, de Boer and others (1980) suggested a northwest-trending Iba fracture zone, possibly related to differential movement of segments in subduction beneath the Manila trench and Zambales Province. Delfin (1984) mapped a local structure, the Maraunot fault (fig. 1), that is probably an extension of the Iba fracture zone beneath Mount Pinatubo. The Maraunot fault trends N.30°W. and generally follows the trend of the Maraunot River and the thermal springs (now covered by the 1991 deposits) on the northwest flank of the volcano.

A northeast-trending lineament of comparable geomorphic expression, here called the Sacobia lineament, was discovered from SLAR imagery in 1991 (Newhall and others, this volume). Subparallel to the Sacobia lineament and <1 km to its north, having a slightly more northerly trend, was a 3-km-long, northeast-trending fracture that opened across the north face of Mount Pinatubo during the initial explosions in April 1991 (Ewert and others, this volume). Extension across the latter fracture occurred on April 2 but apparently not thereafter; tape measurements of a

[1]Philippine Institute of Volcanology and Seismology
[2]U.S. Geological Survey

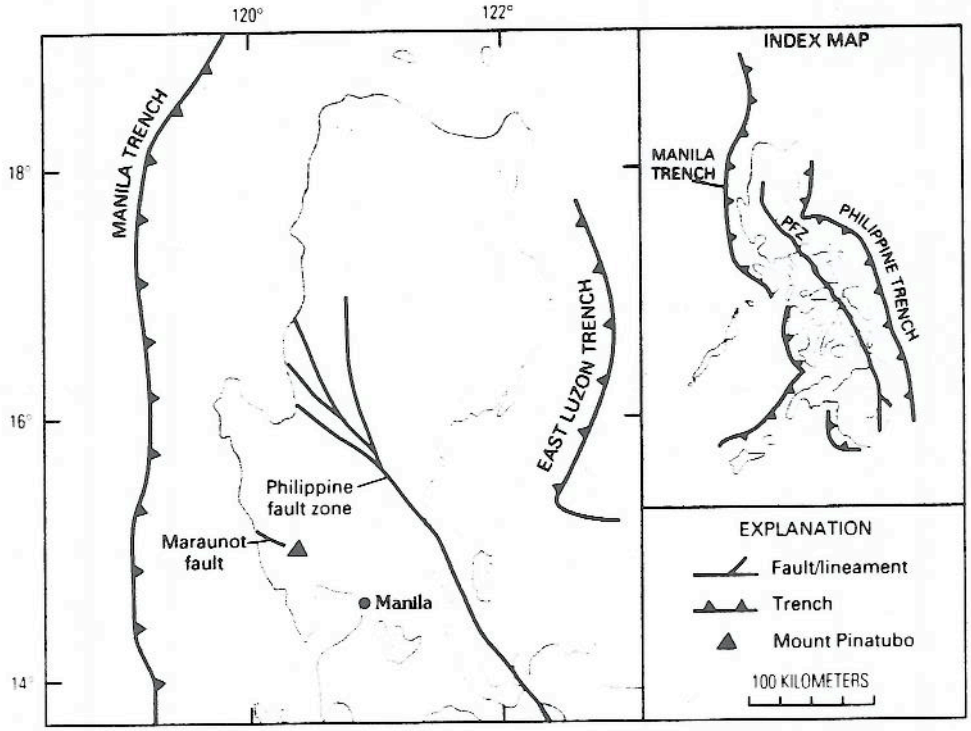

Figure 1. Regional tectonic setting of Mount Pinatubo. PFZ, Philippine fault zone.

quadrilateral across the fracture from May 1 to May 30 did not detect any additional movement along this fracture (Ewert and others, this volume). The Maraunot fault and the Sacobia lineament intersect at Mount Pinatubo.

Delfin (1984) described a subcircular caldera that fully enclosed the pre-1991 Pinatubo dome. The caldera, now termed the Tayawan caldera, measures 4.5 km by 3.5 km and is believed to have been formed >35,000 yr B.P. (Newhall and others, this volume). Delfin (1984) postulated that formation of the Tayawan caldera by "piecemeal and chaotic" collapse resulted in an ill-defined caldera wall.

A new, 2.5-km-wide caldera formed during the June 15, 1991, eruption. Clearly, this structure was not involved in preeruption seismicity; it might have been involved in syneruption and posteruption seismicity. Blocks may have collapsed along ring faults, or, alternatively, collapse may have been in such small pieces that no major faults formed.

METHODOLOGY

Earthquakes that occurred in the Pinatubo area during 1991 and 1992 were recorded digitally from the local PHIVOLCS-USGS telemetry network (Murray and others, this volume; Lockhart and others, this volume). The PCEQ picking program of Valdes (1989) was used to obtain the phase arrival times of the events, initial motions of the primary waves (P-waves), and duration and quality of the arrival times. A PC version of the Hypo71 location program (Lee and Lahr, 1975; Lee, 1989) was also utilized to obtain hypocentral locations of events, magnitudes and other parameters such as quality and fitness of the determination, and focal mechanism parameters including take-off angle, azimuth of station, and polarity of the P-wave initial motion.

We plotted hypocentral data on maps and sections, together with digitized topographic and geologic data, in order to determine the spatial distribution of seismicity and possible correlation with local structures in the area. Separate maps were drawn for preeruption seismicity (fig. 2) and various clusters of posteruption seismicity (see fig. 6).

We tried to plot double-couple focal mechanism solutions of individual events but found it difficult to obtain well-constrained focal mechanism solutions, owing to the very small number of seismic stations. Instead, we wrote software (Bautista and Narag, 1992) that will read the print file (PRT) output of Hypo71pc and display composite first-motion plots (upper hemisphere stereographic projection) for every cluster of seismicity. We then used the known fault geometry of Newhall and others (this volume), supplemented by any linear patterns of epicenters, to select the most likely nodal planes.

Uncertainties in composite focal mechanisms are high, because they require an assumption that earthquakes used in the composite originated from the same source region and have similar mechanisms (Rivera and Cisternas, 1990). With small-magnitude earthquakes ($M<2.5$), there is a possibility that events may represent deformation due to complex interaction of small faults and not from deformation caused by the regional stress field (Zoback, 1992). There is also the danger that events with two differing mechanisms

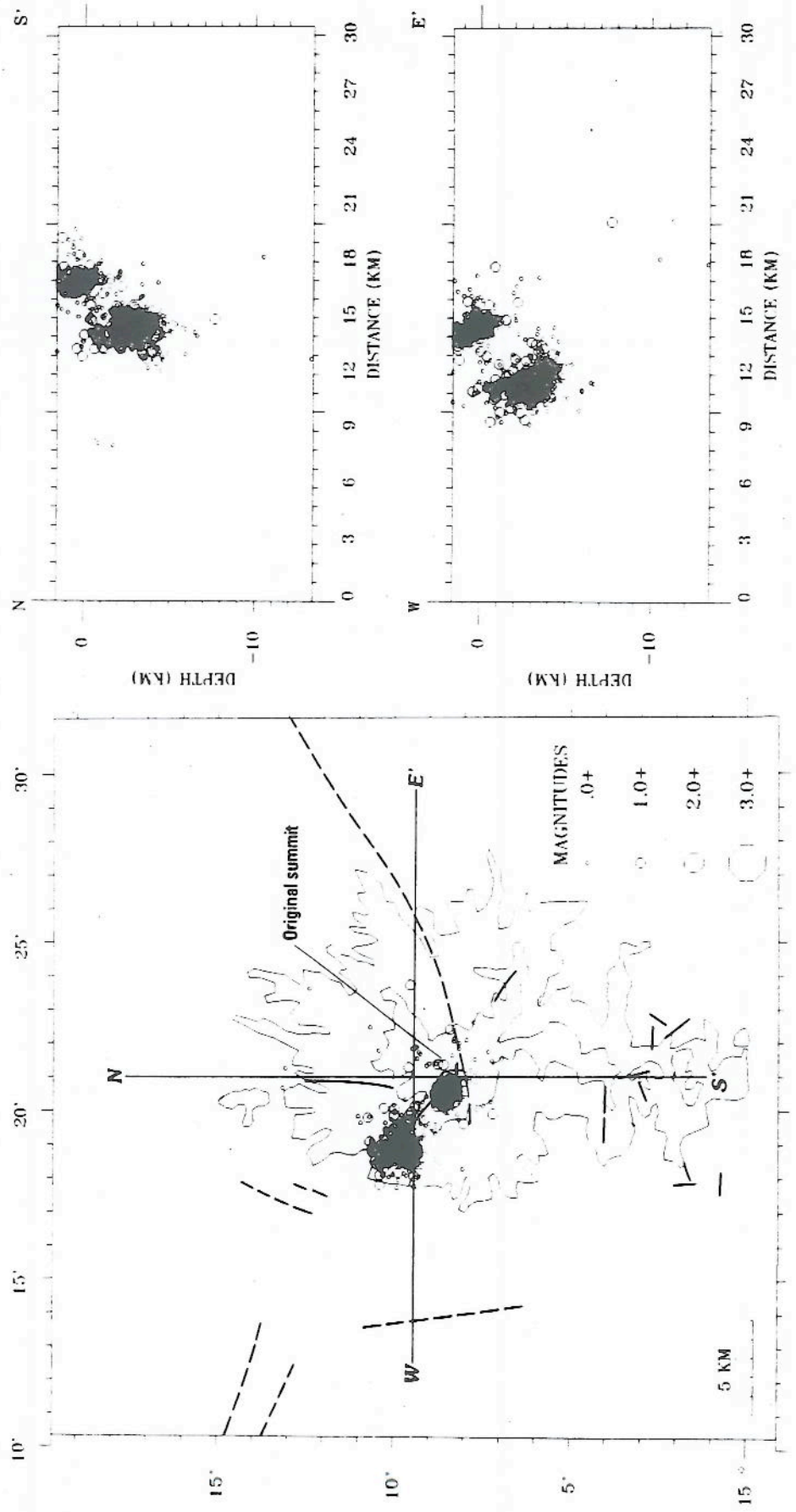

Figure 2. Preeruption seismicity at and near Mount Pinatubo, May 18–June 8, 1991. Events from 0 to 30 km in depth are shown in map view (scale 1:250,000); events from 0 to 15 km in depth are shown in cross sections. Sections show events to 10 km on each side of N–S and E–W. Zero depth indicates sea level. All events shown have RMS≤0.15. Unbroken and broken heavy lines are faults or lineaments from Newhall and others (this volume). Compare with figures 6 and 13.

may be combined and may result in an erroneous third mechanism. We would have preferred, of course, to have had simultaneous recording of single events at many stations and thus to have avoided use of composite mechanisms. However, small events and the limited network were all that we had.

To minimize the previously mentioned uncertainty, we designed plotting software in such a way that the spatial (latitude, longitude, and depth range) and time sampling range can be iteratively varied. This allowed us to observe how the mechanism of events was varying spatially as the sampling window was moved within the cluster being analyzed and also how the mechanism was changing through time. By plotting only events with impulsive first motions, we minimized the possibility of plotting incorrectly read first-motion polarity. Then, to prevent events with erroneous azimuth and take-off angles from obscuring the composite plots, we filtered out events with >1-km horizontal and >2-km vertical errors and >0.5 root mean square (rms) in hypocentral location. Any differences in mechanism between large and small earthquakes were also examined by varying the magnitude range.

The best-fit solutions were then manually correlated with mapped structures and linear features in the distribution of hypocenters, and the most likely nodal planes were selected. The program was then rerun, and events that did not fit the solution were discarded. The inconsistency ratio (Xu and others, 1992), an expression of the fitness of the solution, was then computed. Small inconsistency ratios (<0.3) indicated a reasonably reliable solution. Theoretical analysis of stress change at Mount Pinatubo resulting from the 1990 Luzon earthquake was by the method of Stein and others (1992).

LUZON EARTHQUAKE AFTERSHOCKS NEAR PINATUBO

Most aftershocks of the Luzon earthquake were concentrated north and northwest of the epicenter, and only six apparent aftershocks are known to have occurred in the Pinatubo area (table 1) (Bautista and others, 1992). A few hours after the M_s 7.8 mainshock of the July 16, 1990, Luzon earthquake, an M 4.8 "aftershock" occurred about 10 km southeast of Pinatubo's summit dome. The precise location is not known; uncertainty in National Earthquake Information Center (NEIC) locations for this area is about ±15 km (W. Person, USGS, oral commun., 1991). During the following days, several other earthquakes were recorded and felt around the volcano (table 1). Three weeks later, a nun who was working with the Aeta minority group of Zambales reported rumbling sounds and a landslide measuring about 2–3 ha on the upper northwest face of the volcano (Sabit and others, this volume). The rumbling sounds and landslide were attributed to aftershocks of the tectonic earthquake (Ramos and Isada, 1990). However, the geographic distance of events in table 1 from the mainshock and from most other aftershock activity suggests, alternatively, that they might have been earthquakes akin to those triggered in distant volcanic areas by the M 7.4 Landers earthquake, apparently by transient interaction of seismic waves and previously stressed faults, especially in the presence of pore water or magma (Hill and others, 1993).

Table 1. List of earthquakes around Mount Pinatubo area immediately after the July 16, 1990, Luzon earthquake.

[Local time = G.m.t. + 8 h; NEIC, National Earthquake Information Center, USGS, Denver, Colo.; PHIVOLCS, Philippine Institute of Volcanology and Seismology, Quezon City, Philippines; 33 km is a NEIC default for crustal depths]

Date	Time (G.m.t.)	Coordinates (lat/long)	Magnitude	Depth (km)	Data source
7/16/90	0825	15.46N/120.76E	4.6	33	NEIC
7/16/90	1015	15.11N/120.41E	4.8	33	NEIC
7/22/90	0221	15.38N/120.61E	4.3	33	NEIC
7/23/90	2025	15.39N/120.63E	3.0	6	PHIVOLCS
8/8/90	1938	15.16N/120.52E	4.4	10	NEIC
8/26/90	1058	15.29N/120.40E	3.6	6	PHIVOLCS

COMPOSITE FOCAL MECHANISMS

PREERUPTION SEISMICITY

In early April 1991, in response to reports of unusual activity, PHIVOLCS installed a small network consisting of four portable digital seismographs and found an epicentral cluster located approximately 6 km northwest of the summit dome (Sabit and others, this volume). A network of 7 telemetered seismometers was installed during late April and the first week of May (Lockhart and others, this volume), and results from the first month of telemetry data confirmed the same northwest cluster (Power and others, this volume; Harlow and others, this volume) (fig. 2). Then, from May 27 to June 5, 1991, another cluster of hypocenters developed 1 to 4 km below the volcano summit (fig. 2). Seismic activity in the northwest cluster slowed but did not stop entirely. Meanwhile, seismicity below the summit intensified (Power and others, this volume; Harlow and others, this volume).

A comparison of focal mechanisms from the northwest and summit clusters could help us understand their origins and explain why only the summit cluster culminated in an eruption. Figure 3 is a composite first-motion plot for events of the northwest cluster, excluding those with emergent onsets and those whose solutions did not fit a preliminary match of solutions and known faults. The sampling window and other parameters used in the plots are displayed at the left of the figure. Because this cluster bisected by the northwest-trending Maraunot fa-

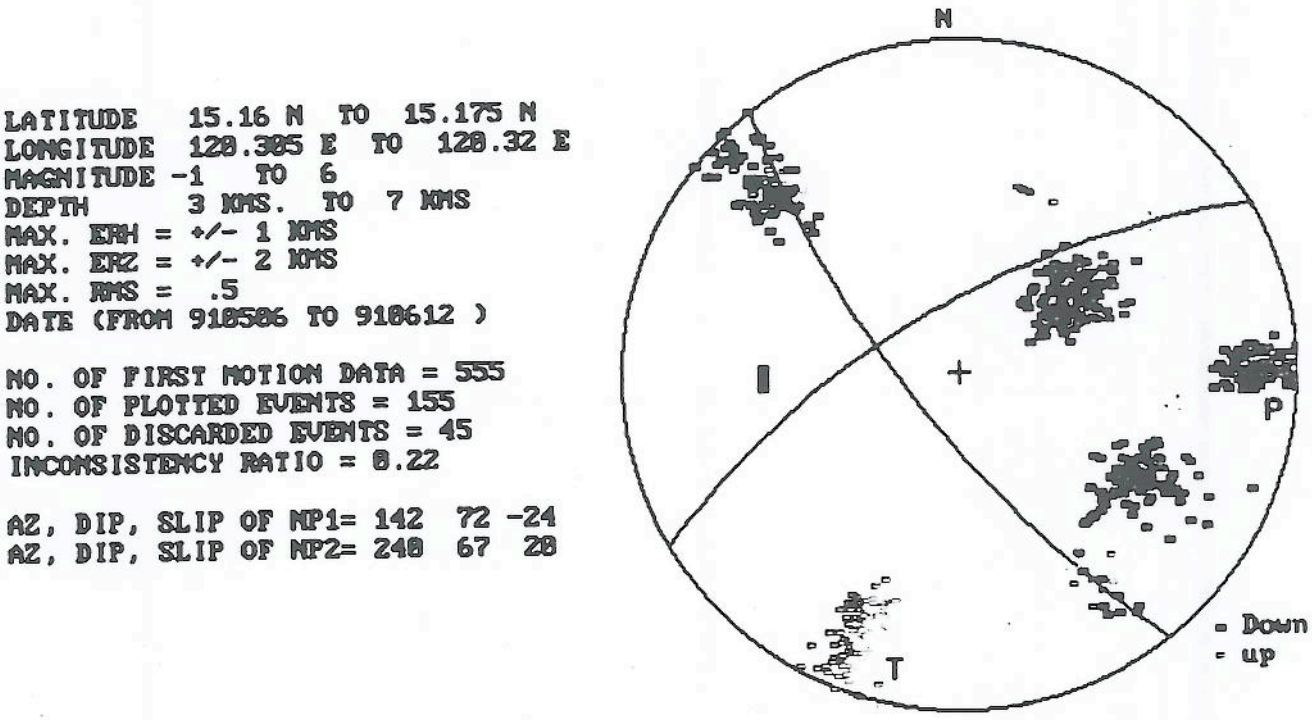

Figure 3. Focal mechanism solutions for 155 preeruption earthquakes in the northwest cluster (see fig. 2). Plots are upper hemisphere stereographic projections. P, axis of maximum compressional stress; T, axis of minimum compressional (maximum tensional) stress. N, geographic north. NP1, first nodal plane; NP2, second nodal plane; ERH, horizontal error; ERZ, vertical error; RMS, root mean square.

(Delfin,1984: Delfin and others, this volume), we constrained the first nodal plane (NP1) in figure 3 to be parallel to the fault trend (azimuth about 142°), with a steep trial dip of 72° northeast. Interestingly, the plane cuts through the two clusters of station first-motion plots with highly mixed polarities. Mixed polarities are commonly observed when the location of the station is aligned with the trend of the causative fault. However, points outside these clusters have either negative or positive first motions, in an interpretable pattern. Tentatively, we infer left-lateral strike slip along the northwest-trending Maraunot fault, with the maximum and minimum stress axes oriented east-west and north-south, respectively.

Figure 4 is a plot for the summit cluster. In figure 4, all six station clusters showed highly mixed first-motion polarities. Thus, events of the summit cluster have diverse mechanisms, which are characteristic of earthquakes resulting from magmatic intrusion.

SYNERUPTION SEISMICITY

The major explosive eruptions of Mount Pinatubo started on June 12 and peaked on June 15. Starting June 12, the remote stations of the seismic network began to fail from thick ash fall and pyroclastic flows. Only two seismographs on Pinatubo's east slope (PIEZ and CABZ) remained in operation until the start of the climactic eruption on June 15, and, by 1415 on June 15, only CABZ remained.

Starting at about 1530 on June 15, quakes began to be felt one after another at Magalang, Pampanga, located about 30 km east of the volcano. Signals recorded by most of PHIVOLCS national seismic stations were saturated with eruption signals and thus failed to give good P-wave arrival data for epicentral or first-motion determinations. Fortunately, the NEIC was able to determine the epicenters of 32 events during the June 15–16 period by using data from participating seismic stations in the world, including those from the Philippines. All events could have been within 40 km of Mount Pinatubo. The biggest of the June 15 events occurred at 1915 (M_b 5.5).

NEIC determined focal mechanisms of the seven largest events (1539, 1841, 1911, 1915, and 2025 on June 15; 0348 and 0358 on June 16). Six of these events (all but that at 0348 on June 16) had predominantly strike-slip movement (fig. 5) with a minor vertical (normal or reverse) component. The event at 0348 on June 16, however, was normal faulting with a large strike-slip component. All events were poorly constrained because of the sparsity of the data and because first-motion reports were mostly emergent in nature. In addition, for NEIC to make reliable teleseismic fault-plane solutions, earthquakes generally need to have magnitudes of at least 5.8.

These results, although poorly constrained, suggest that the largest quakes on June 15 were strike-slip events

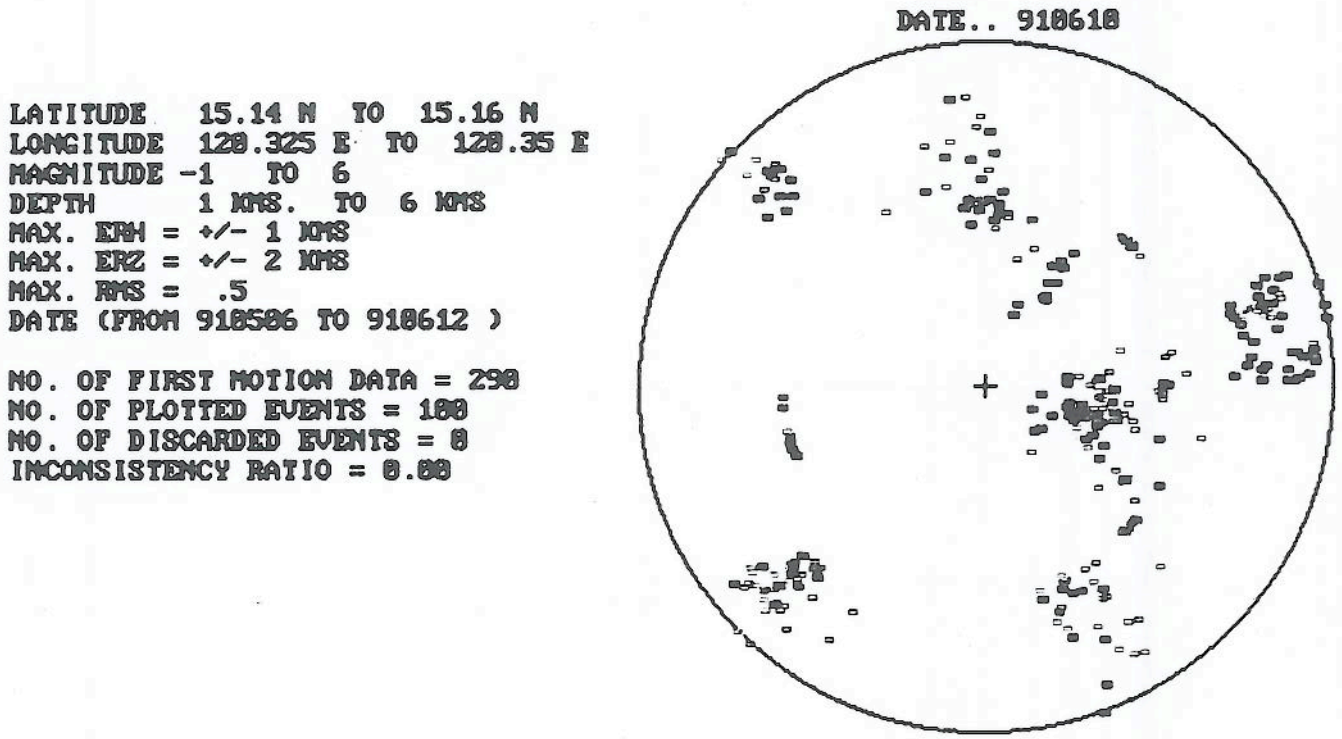

Figure 4. First-motion plots for 100 preeruption earthquakes in the summit cluster (see fig. 3). Upper hemisphere projections; conventions as in figure 3. Emergent first-motions removed. No consistent focal mechanism determined.

consistent with the east-west maximum regional stress. This also implies that regional tectonic adjustments accompanied and immediately followed the caldera-forming eruption. Apparently, tectonic adjustments occurred in response to the abrupt drop in pressure inside the magma chamber.

Contrary to our interpretation at the time and some interpretations elsewhere (for example, Filson and others, 1973; Hirn and others, 1991), the largest earthquakes were not due to caldera collapse. Among the largest earthquakes, only the 0348 event on June 16 might have been a collapse event, but independent stratigraphic evidence (W.E. Scott and others, this volume) suggests that collapse began in the late afternoon of June 15. However, there were also many smaller earthquakes that were difficult to locate and whose first motions are difficult to decipher because of an emergent character of the waveform, and some of these quakes could have been associated with caldera collapse.

POSTERUPTION SEISMICITY

After restoration of the seismic telemetry network (by June 29), we noticed a shift in locations of seismicity relative to preeruption sources. Earthquakes were distributed over a wide area outside and away from the active volcanic center (Mori, White, and others, this volume). Seven prominent posteruption earthquake clusters, labeled A–F, are shown in figure 6.

Cluster A—Northwest Cluster.—A cluster of earthquakes (A, fig. 6) occurred northwest of Mount Pinatubo but slightly south and deeper than the preeruption northwest cluster. We cannot say whether this shift is real or is due to the change in the configuration of the newly restored network. However, the large change in the hypocentral range and the presence of a deeper clusters of hypocenters suggest to us that the shift was real and that earthquakes were occurring in a new source zone.

The absence of a station northwest of Pinatubo in the new network increased uncertainty in first-motion solutions, especially that for cluster A. Of several solutions that we tried, that which gave the lowest inconsistency ratio (fig. 7) has one nodal plane bisecting the two first-motion clusters with mixed polarities and implies strike-slip motion with a moderate amount of normal slip. The maximum stress axis is oriented east-northeast. Mechanisms of earthquakes with $M<1$ gave the same solution as those with $M>1$.

Cluster B—Summit Cluster.—The preeruption summit cluster was still present after the eruption but was tightly concentrated in a small area close to the southwest rim of the new caldera (B, fig. 6). Figure 8 is the first-motion plot for the posteruption summit cluster. As during the preeruption period, the earthquakes in this cluster show very diverse mechanisms, and no predominant mechanism can be recognized from the first-motion plot.

Cluster C—East-northeast Cluster.—The most pronounced cluster of all (C, fig. 6), developed 2 to 3 km east-northeast of the new caldera between 0 and 5 km depth. This cluster completely masked the location of the northern trace of the Tayawan caldera, the northeast-trending fracture zone that formed on April 2, 1991, and that part of the Sacobia lineament (Newhall and others, this volume) that is just northeast of the 1991 caldera.

Starting August 25 (and especially after September 9), 1991, there was a noticeable shift in the polarity of first motions at several stations that suggests a change of mechanism. In figure 9*A*, we eliminated all events after this shift and found a strike-slip solution with east-west compression. After August 25, the solution shifted slightly (fig. 9*B*).

The above results indicate that right-lateral movement along one or more northeast-trending faults was responsible for this cluster. Some of that movement might have been along the fracture that opened on April 2, 1991, but it is unclear why there was no seismicity along this feature between April 5 and the June eruptions. Alternatively, movement might have been along the Sacobia lineament (fig. 6).

Cluster D—Southeast Cluster.—About 5 km southeast of the 1991 caldera rim, another dense cluster extends from 7 to 15 km in depth (D, fig. 6). If we view this cluster in east-west cross section, as is also shown in figure 6, the outwardly dipping structure resembles a dike that, if projected toward the surface, intersects the southeast trace of the Tayawan caldera. If this activity is related to the movement along the old caldera ring fracture, it apparently was limited to a short segment of that ring fracture, unlike movement along the whole ring structure of Rabaul caldera, Papua New Guinea (McKee and others, 1984; Mori and McKee, 1986). The focal mechanism for this cluster is not well constrained but is probably normal faulting with a small strike-slip component (fig. 10*A*) or pure normal faulting (fig. 10*B*). Choosing nodal plane 1 in figure 10B as the fault plane (strike 195°, dip 60°W.) will make it consistent with the spatial trend of the earthquake cluster.

Cluster E—South-southeastern Cluster.—Another prominent cluster is located approximately 7 km south-southeast of the 1991 caldera, in the shallow depth range of 0 to 4 km (E, fig. 6). There are at least three possible solutions for this cluster. One possible solution is a strike-slip mechanism (fig. 11*A*) with P-axis oriented east-west. The second solution (fig. 11*B*) is movement along an east-northeast striking normal fault. The third solution (fig. 11*C*) is also along a normal fault, but this time the strike is north-northeast. We have no basis on which to choose any one of these solutions over another, except to say that the first is the most consistent with mechanisms observed in other clusters.

Cluster F—Northeast, Clark Air Base Cluster.—The Clark Air Base cluster (F, fig. 6) consists of events that were scattered along a northeast-trending elongate area about 15 km northeast of the summit. Most of the earthquakes in this cluster were felt at the Pinatubo Volcano Observatory on Clark Air Base. Figure 12 shows a strike-slip solution with maximum stress axis oriented close to east-west. The above result suggests right-lateral movement along a northeast-trending fault, probably that seen as a strong lineament in SLAR imagery of the Sacobia River (fig. 4 of Newhall and others, this volume).

Starting in January 1992, the character of seismicity at Pinatubo changed (fig. 13). The activity in some of the clusters that were very active in 1991 diminished. In contrast, the seismicity at the summit cluster further intensified before and during growth of a dome in July–October 1992 (Ramos and others, this volume), and again at the time of this writing (February–May 1994).

THEORETICAL ANALYSIS OF STRESS CHANGE RESULTING FROM 1990 LUZON EARTHQUAKE

The magnitude of stress changes resulting from the Luzon earthquake is shown in figure 14 (Coulomb stress change). For an assumed coefficient of friction of 0.4, the rise in Coulomb stress would have been between 0.1 and 0.2 bar along optimally oriented faults of the Pinatubo area (thrust faults striking north-south and dipping 25–35°E. or 30–40°W.; vertical strike-slip faults striking N.25–35°E. and N.25–35°W. This is one order of magnitude higher than tidal stress and somewhat lower than that thought to have triggered aftershocks of the Landers earthquake at a comparable distance (Stein and others, 1992).

In contrast, volumetric stress change (fig. 15) would have subjected Pinatubo to a 1-bar increase in compressive stress. This is about 50 times the daily tidal pressure change.

Were such changes in Coulomb or volumetric stress sufficient to trigger magma ascent beneath Pinatubo? We know of no well-defined threshold of stress change that can be said to trigger magma ascent. Empirically, there are a number of instances of eruptions shortly after large regional earthquakes (some are listed in Newhall and Dzurisin, 1988), so we think that a threshold can, apparently, be exceeded. We can imagine that an increase in compressive stress might have squeezed magma upward, either from the main reservoir into the overlying volcanic edifice or from a deeper, possibly disseminated reservoir of basaltic magma into the base of the main dacitic body. The first of these cases was suggested by Nakamura (1971), though questioned by Rikitake and Sato (1989). The small diameter of Pinatubo's conduit (approximately 100 m; Hoblitt, Wolfe, and others, this volume) relative to the diameter of the magma reservoir (about 5 km, Mori, Eberhardt-Phillips, and

6/15/91 LUZON, PHILIPPINE IS.
07:39:09.5 5.1 mb

	AZIMUTH	PLUNGE
P axis	75.2	18.8
T axis	171.3	17.3
B axis	301.0	64.0
X axis	123.5	26.0
Y axis	33.0	1.0
123.00	89.00	-26.00
213.49	64.00	-178.89

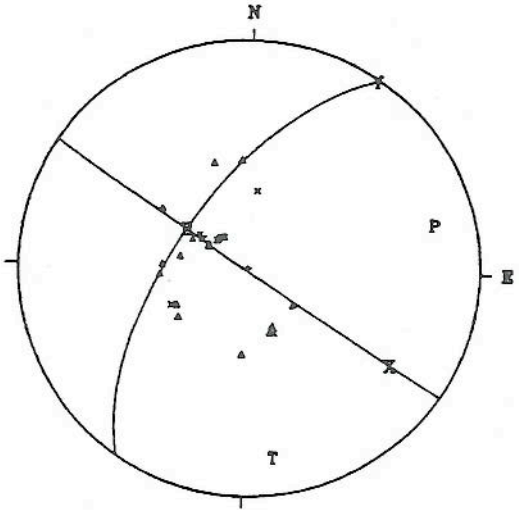

6/15/91 LUZON. PHILIPPINE IS.
10:41:14.2 5.5 mb

	AZIMUTH	PLUNGE
P axis	263.9	4.2
T axis	171.9	26.0
B axis	2.4	63.8
X axis	221.0	21.2
Y axis	125.0	15.0
215.00	75.00	158.00
310.97	68.76	16.12

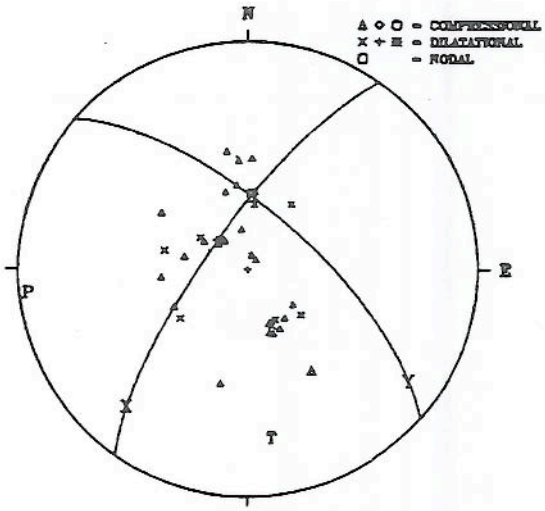

6/15/91 LUZON,PHILIPPINE IS.
11:11:18.4 5.0 mb

	AZIMUTH	PLUNGE
P axis	262.7	1.6
T axis	172.0	23.2
B axis	356.5	66.7
X axis	219.8	17.4
Y axis	125.0	15.0
215.00	75.00	162.00
309.81	72.63	15.73

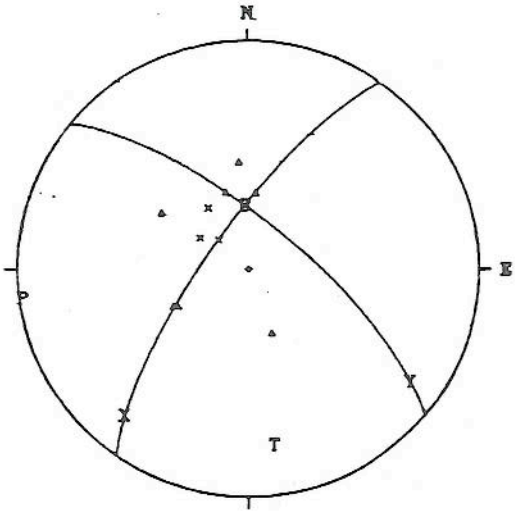

6/15/91 LUZON, PHILIPPINE IS..
11:15:28.0 5.7 mb

	AZIMUTH	PLUNGE	AZIMUTH	PLUNGE
P axis	263.9	4.2	99.0	0.0
T axis	171.9	26.0	9.0	0.0
B axis	2.4	63.6	0.0	90.0
X axis	221.0	21.2	54.0	0.0
Y axis	125.0	15.0	144.0	0.0

215.00	75.00	158.00	234.00	90.00	-180.00
310.97	68.79	16.12	324.00	90.00	0.00

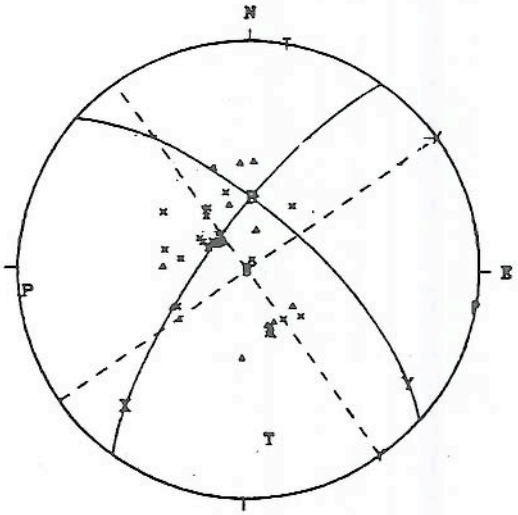

6/15/91 LUZON, PHILIPPINE IS.
12:25:30.4 5.0 mb

	AZIMUTH	PLUNGE
P axis	85.1	1.6
T axis	176.2	34.7
B axis	352.9	55.2
X axis	226.1	22.5
Y axis	125.0	25.0

215.00	65.00	155.00
316.15	67.48	27.23

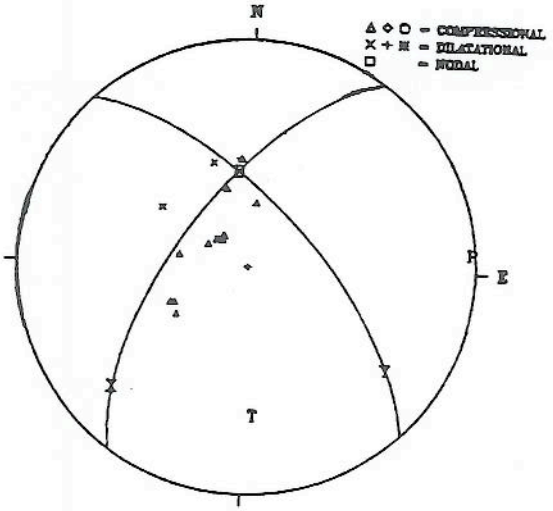

6/15/91 LUZON. PHILIPPINE IS.
19:48:53.5 5.0 mb

	AZIMUTH	PLUNGE
P axis	94.0	50.8
T axis	330.8	24.1
B axis	226.5	28.9
X axis	13.9	56.8
Y axis	128.0	15.0

218.00	75.00	-120.00
103.85	33.23	-28.19

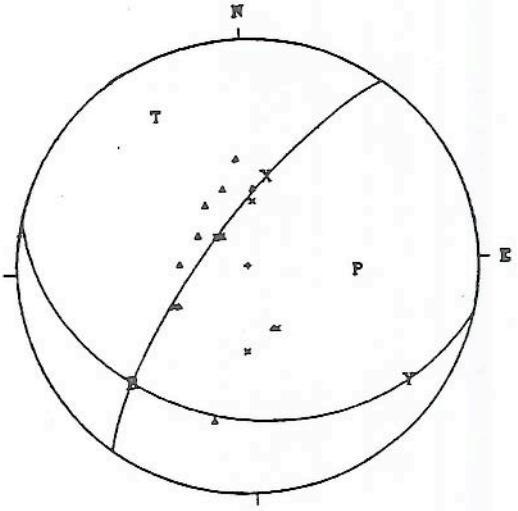

6/15/91 LUZON,PHILIPPINE IS.
19:58:35.1 4.9 mb

	AZIMUTH	PLUNGE
P axis	76.7	16.1
T axis	170.2	12.0
B axis	295.3	69.8
X axis	33.0	2.8
Y axis	124.0	20.0

214.00	70.00	183.00
122.97	87.18	339.97

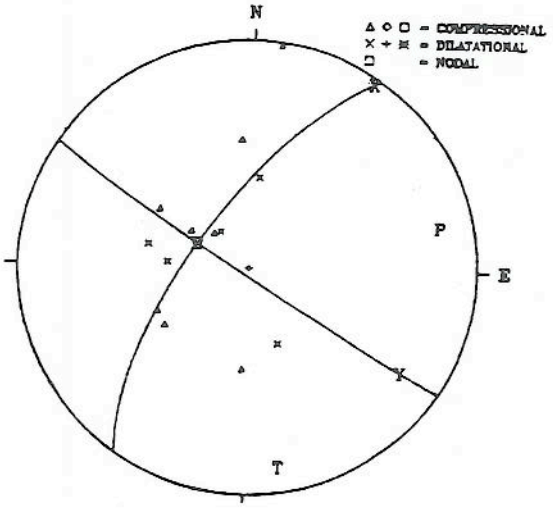

Figure 5. Focal mechanism solutions for seven syneruption earthquakes. Data and solutions from National Earthquake Information Center, USGS. Times are G.m.t.; local time=G.m.t. plus 8 h. Except for the event at 1948 G.m.t., all other events were strike-slip events along northwest- or northeast-trending faults.

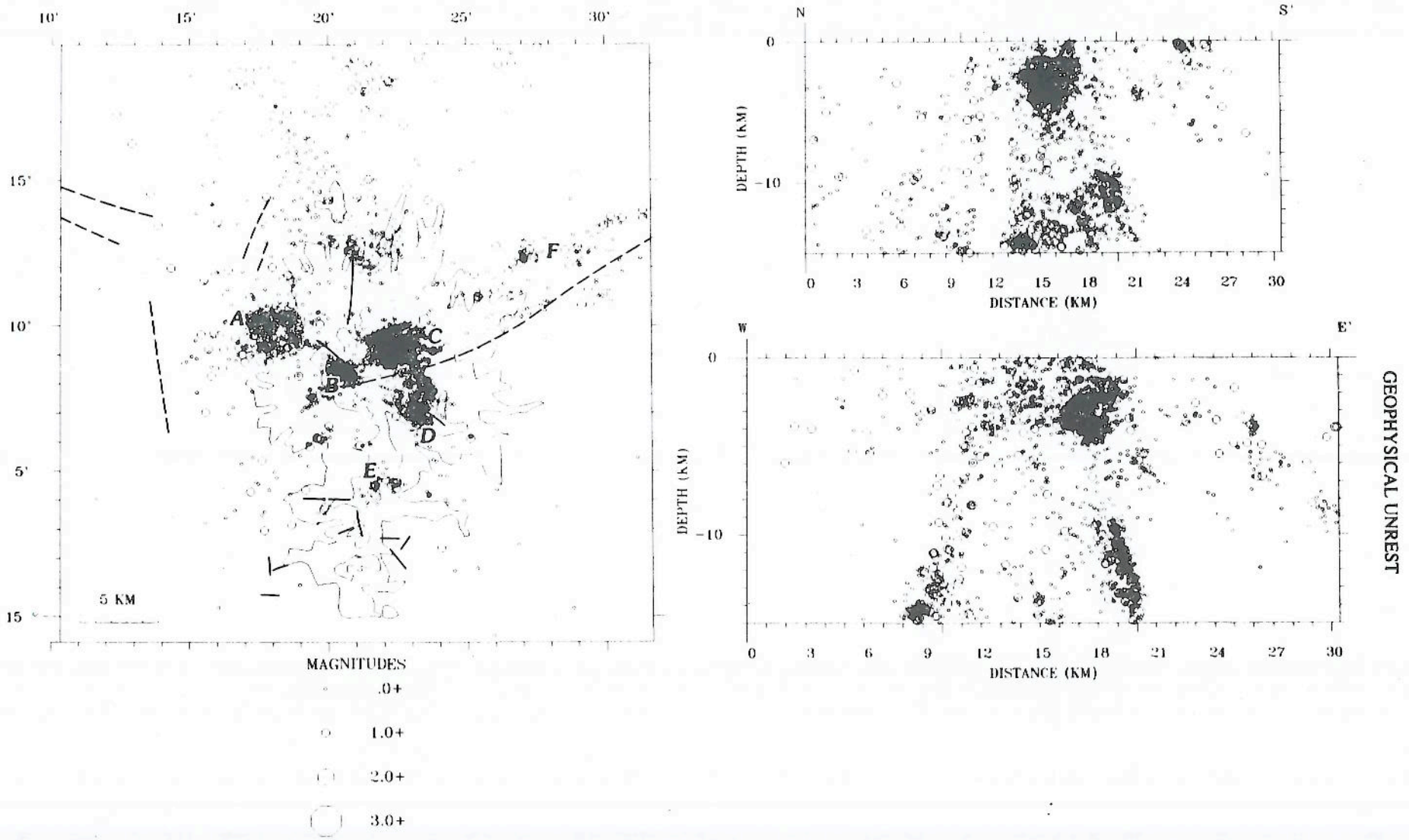

Figure 6. Posteruption seismicity at and near Mount Pinatubo, June 26 to August 19, 1991. Events from 0 to 30 km in depth are shown in map view; events from 0 to 15 km in depth are shown in cross sections. Zero depth is at the vent. All events shown have RMS≤0.15. Heavy lines are faults or lineaments from Newhall and others (this volume). Six clusters, labeled A–F, are described individually in the text and in figures 7–12. Cross sections are shown in figure 2.

```
LATITUDE   15.15 N  TO  15.17 N
LONGITUDE  120.275 E  TO  120.325 E
MAGNITUDE -1   TO  6
DEPTH      5 KMS.  TO  15 KMS
MAX. ERH = +/- 1 KMS
MAX. ERZ = +/- 2 KMS
MAX. RMS =  .5
DATE (FROM 910627 TO 911231 )

NO. OF FIRST MOTION DATA = 511
NO. OF PLOTTED EVENTS = 98
NO. OF DISCARDED EVENTS = 0
INCONSISTENCY RATIO = 0.00

AZ, DIP, SLIP OF NP1= 195  85  45
AZ, DIP, SLIP OF NP2= 100  45 -7
```

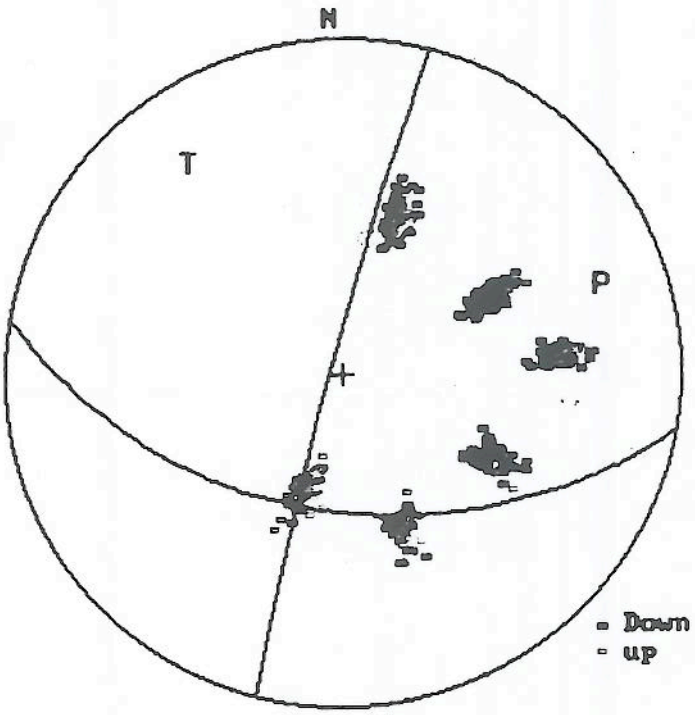

Figure 7. Focal mechanism solutions for posteruption cluster A. Conventions as in figure 3.

```
LATITUDE   15.125 N  TO  15.15 N
LONGITUDE  120.325 E  TO  120.36 E
MAGNITUDE -1   TO  6
DEPTH      1 KMS.  TO  6 KMS
MAX. ERH = +/- 1 KMS
MAX. ERZ = +/- 2 KMS
MAX. RMS =  .5
DATE (FROM 910626 TO 911231 )

NO. OF FIRST MOTION DATA = 374
NO. OF PLOTTED EVENTS = 83
NO. OF DISCARDED EVENTS =
INCONSISTENCY RATIO =
```

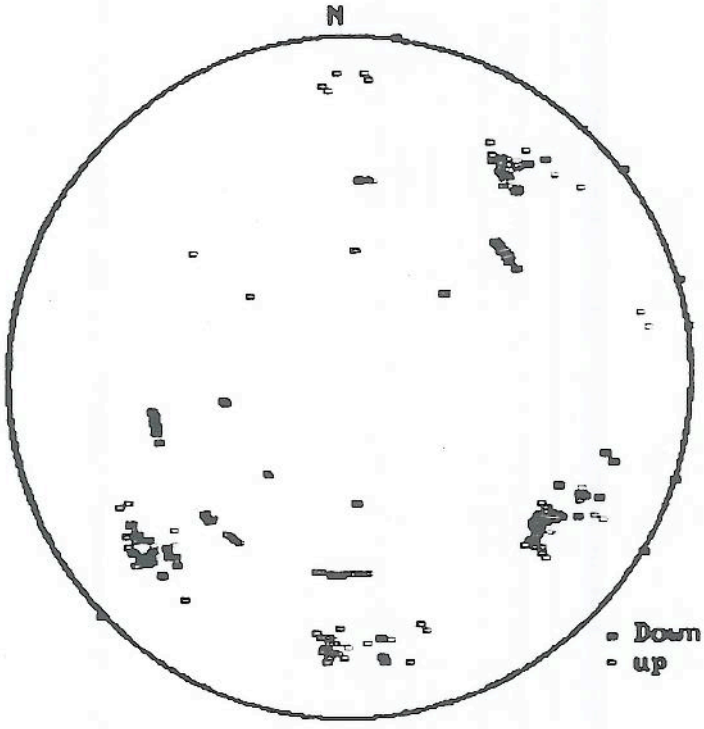

Figure 8. First-motion plot for posteruption cluster B. Conventions as in figure 3. No consistent mechanism emerged.

```
LATITUDE   15.075 N  TO  15.11 N
LONGITUDE  120.35 E  TO  120.375 E
MAGNITUDE -1   TO  6
DEPTH      1 KMS.  TO  6 KMS
MAX. ERH = +/- 1 KMS
MAX. ERZ = +/- 2 KMS
MAX. RMS =  .5
DATE (FROM 910626 TO 911231 )

NO. OF FIRST MOTION DATA = 246
NO. OF PLOTTED EVENTS = 42
NO. OF DISCARDED EVENTS = 0
INCONSISTENCY RATIO = 0.00

AZ, DIP, SLIP OF NP1= 220  40  15
AZ, DIP, SLIP OF NP2= 120  80 -45
```

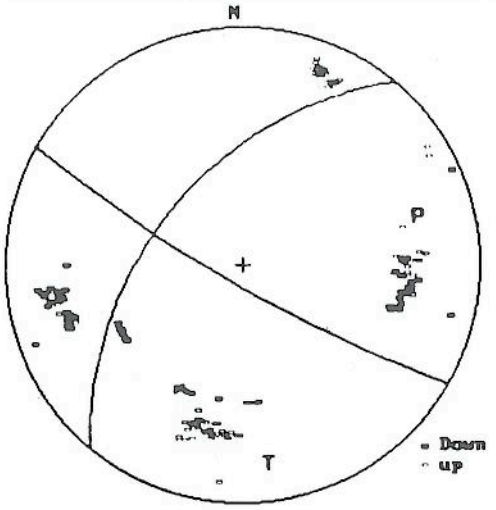


```
LATITUDE   15.075 N  TO  15.11 N
LONGITUDE  120.35 E  TO  120.375 E
MAGNITUDE -1   TO  6
DEPTH      1 KMS.  TO  6 KMS
MAX. ERH = +/- 1 KMS
MAX. ERZ = +/- 2 KMS
MAX. RMS =  .5
DATE (FROM 910626 TO 911231 )

NO. OF FIRST MOTION DATA = 248
NO. OF PLOTTED EVENTS = 41
NO. OF DISCARDED EVENTS = 0
INCONSISTENCY RATIO = 0.00

AZ, DIP, SLIP OF NP1= 85  30  90
AZ, DIP, SLIP OF NP2= 265  60 -90
```

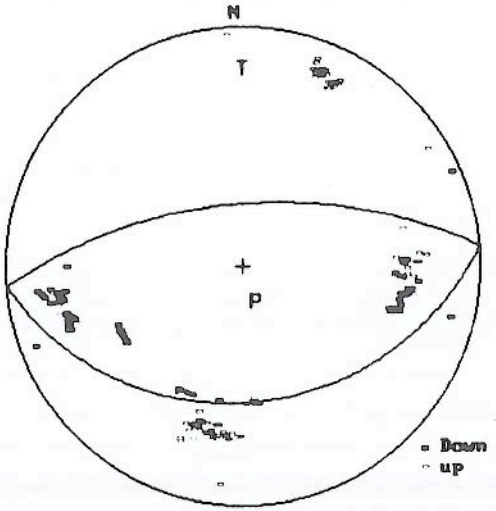

Figure 11. Three possible focal mechanism solutions (*A*, *B*, and *C*) for posteruption cluster F. Conventions as in figure 3. None are well constrained; the strike-slip solution in figure 12*A* is the most consistent with mechanisms observed in other clusters.


```
LATITUDE   15.075 N  TO  15.11 N
LONGITUDE  120.35 E  TO  120.375 E
MAGNITUDE -1   TO  6
DEPTH      1 KMS.  TO  6 KMS
MAX. ERH = +/- 1 KMS
MAX. ERZ = +/- 2 KMS
MAX. RMS =  .5
DATE (FROM 910626 TO 911231 )

NO. OF FIRST MOTION DATA = 246
NO. OF PLOTTED EVENTS = 42
NO. OF DISCARDED EVENTS = 0
INCONSISTENCY RATIO = 0.00

AZ, DIP, SLIP OF NP1= 15  25  90
AZ, DIP, SLIP OF NP2= 195  65 -90
```

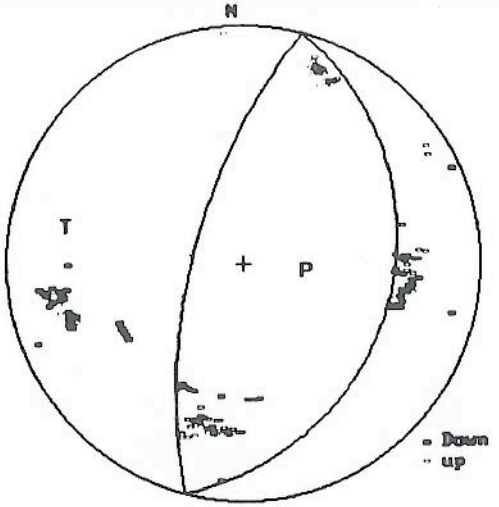

Figure 11.—Continued.

```
LATITUDE   15.18 N  TO  15.22 N
LONGITUDE  120.44 E  TO  120.46 E
MAGNITUDE -1   TO  6
DEPTH      4 KMS.  TO  10 KMS
MAX. ERH = +/- 2 KMS
MAX. ERZ = +/- 3 KMS
MAX. RMS =  .5
DATE (FROM 900101 TO 931230 )

NO. OF FIRST MOTION DATA = 83
NO. OF PLOTTED EVENTS = 23
NO. OF DISCARDED EVENTS = 18
INCONSISTENCY RATIO = 0.44

AZ, DIP, SLIP OF NP1= 60  90  72
AZ, DIP, SLIP OF NP2= 330  70  0
```

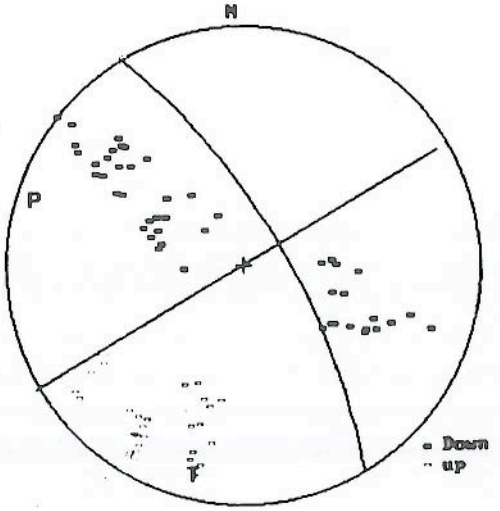

Figure 12. Focal mechanism solutions for posteruption cluster F. Conventions as in figure 3.

LATITUDE 15.145 N TO 15.175 N
LONGITUDE 120.38 E TO 120.4 E
MAGNITUDE -1 TO 6
DEPTH 4 KMS. TO 8 KMS
MAX. ERH = +/- 1 KMS
MAX. ERZ = +/- 2 KMS
MAX. RMS = .5
DATE (FROM 918626 TO 918825)

NO. OF FIRST MOTION DATA = 186
NO. OF PLOTTED EVENTS = 27
NO. OF DISCARDED EVENTS = 0
INCONSISTENCY RATIO =

AZ, DIP, SLIP OF NP1= 325 75 19
AZ, DIP, SLIP OF NP2= 230 70 -14

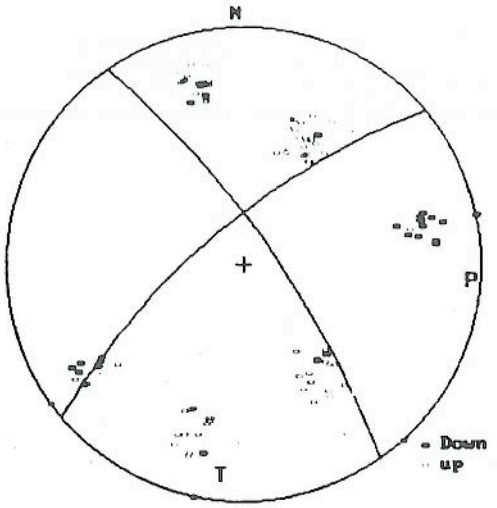

LATITUDE 15.145 N TO 15.175 N
LONGITUDE 120.38 E TO 120.4 E
MAGNITUDE -1 TO 6
DEPTH 4 KMS. TO 8 KMS
MAX. ERH = +/- 1 KMS
MAX. ERZ = +/- 2 KMS
MAX. RMS = .5
DATE (FROM 918825 TO 911231)

NO. OF FIRST MOTION DATA = 354
NO. OF PLOTTED EVENTS = 68
NO. OF DISCARDED EVENTS = 0
INCONSISTENCY RATIO =

AZ, DIP, SLIP OF NP1= 338 55 0
AZ, DIP, SLIP OF NP2= 68 90 72

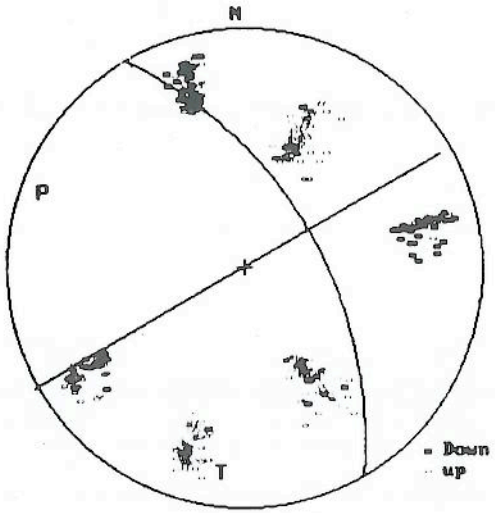

Figure 9. First-motion and focal mechanism plots for posteruption cluster C. Conventions as in figure 3. *A*, Events from June 26 to August 25, before an apparent shift in focal mechanisms for this cluster. *B*, Events from August 25 through December 31.

LATITUDE 15.11 N TO 15.125 N
LONGITUDE 120.375 E TO 120.395 E
MAGNITUDE -1 TO 6
DEPTH 5 KMS. TO 15 KMS
MAX. ERH = +/- .5 KMS
MAX. ERZ = +/- 1 KMS
MAX. RMS = .5
DATE (FROM 918626 TO 911231)

NO. OF FIRST MOTION DATA = 380
NO. OF PLOTTED EVENTS = 93
NO. OF DISCARDED EVENTS = 0
INCONSISTENCY RATIO = 0.00

AZ, DIP, SLIP OF NP1= 200 75 61
AZ, DIP, SLIP OF NP2= 85 33 -29

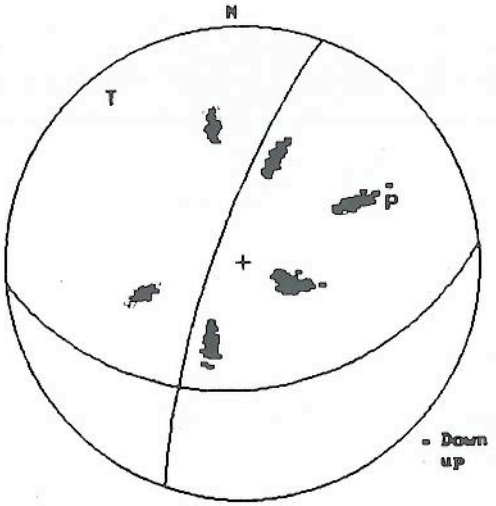

LATITUDE 15.11 N TO 15.125 N
LONGITUDE 120.375 E TO 120.395 E
MAGNITUDE -1 TO 6
DEPTH 5 KMS. TO 15 KMS
MAX. ERH = +/- .5 KMS
MAX. ERZ = +/- 1 KMS
MAX. RMS = .5
DATE (FROM 918626 TO 911231)

NO. OF FIRST MOTION DATA = 380
NO. OF PLOTTED EVENTS = 93
NO. OF DISCARDED EVENTS = 0
INCONSISTENCY RATIO = 0.00

AZ, DIP, SLIP OF NP1= 195 60 -90
AZ, DIP, SLIP OF NP2= 15 30 90

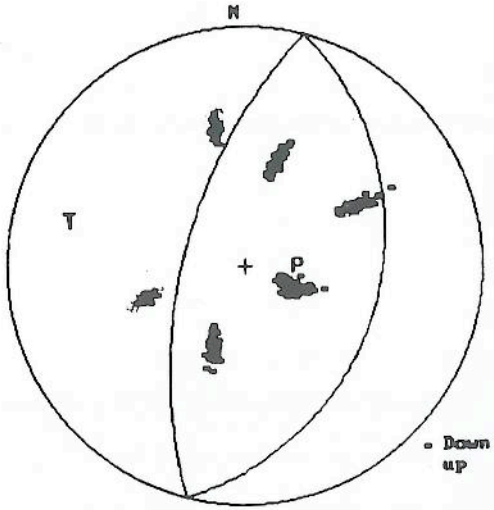

Figure 10. Focal mechanism solutions for posteruption cluster D. Conventions as in figure 3. *A*, All events. *B*, Same as *A* with alternative focal plane solution.

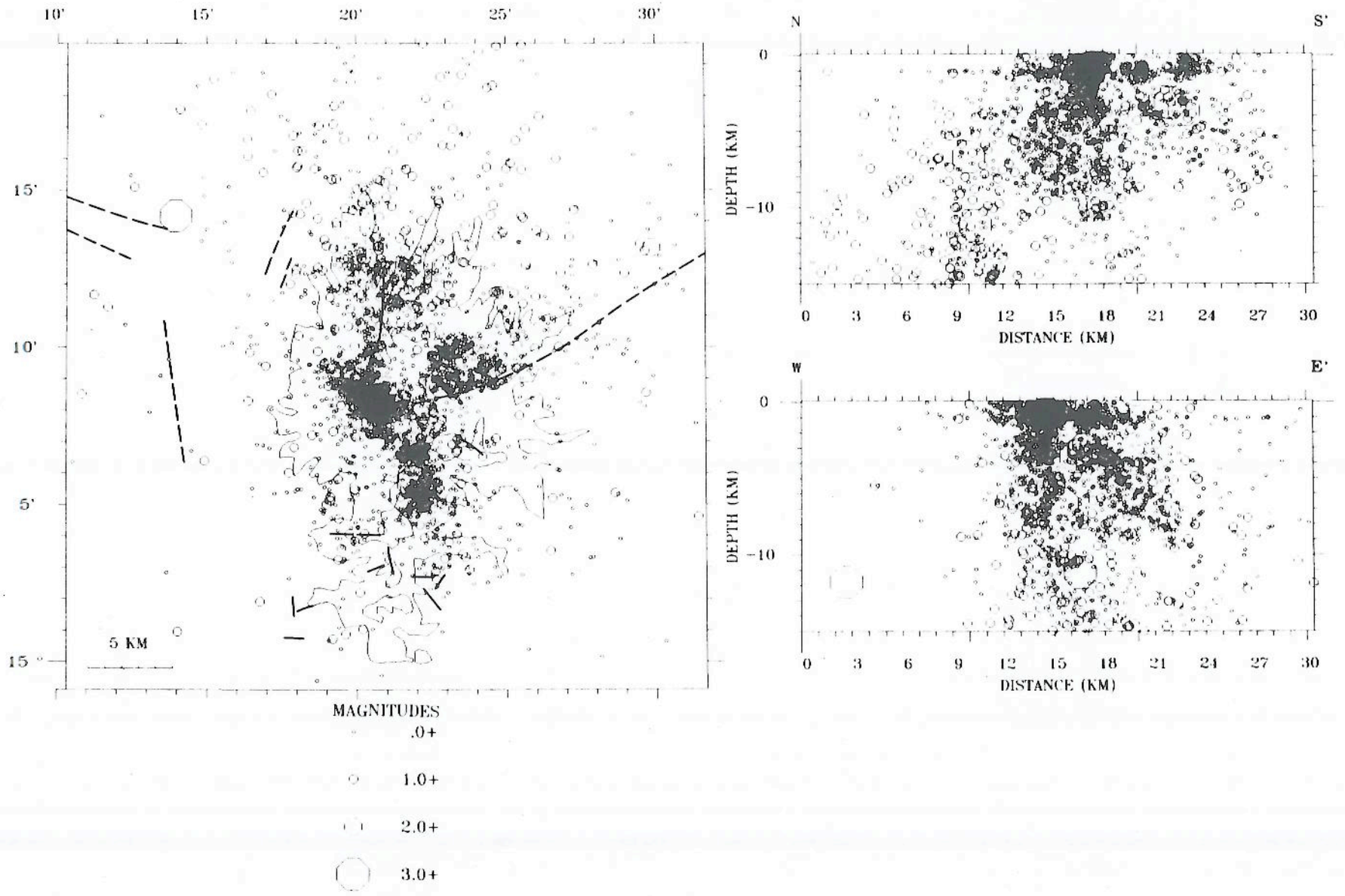

Figure 13. Seismicity at and near Mount Pinatubo, January–December 1992. Events from 0 to 30 km in depth are shown in map view; events from 0 to 15 km in depth are shown in cross sections. Zero depth is at the vent. All events shown have RMS≤0.15. Note that most 1992 seismicity was beneath or near the caldera (associated with renewed dome growth) and in posteruption cluster E (fig. 6). Cross sections are shown in figure 2.

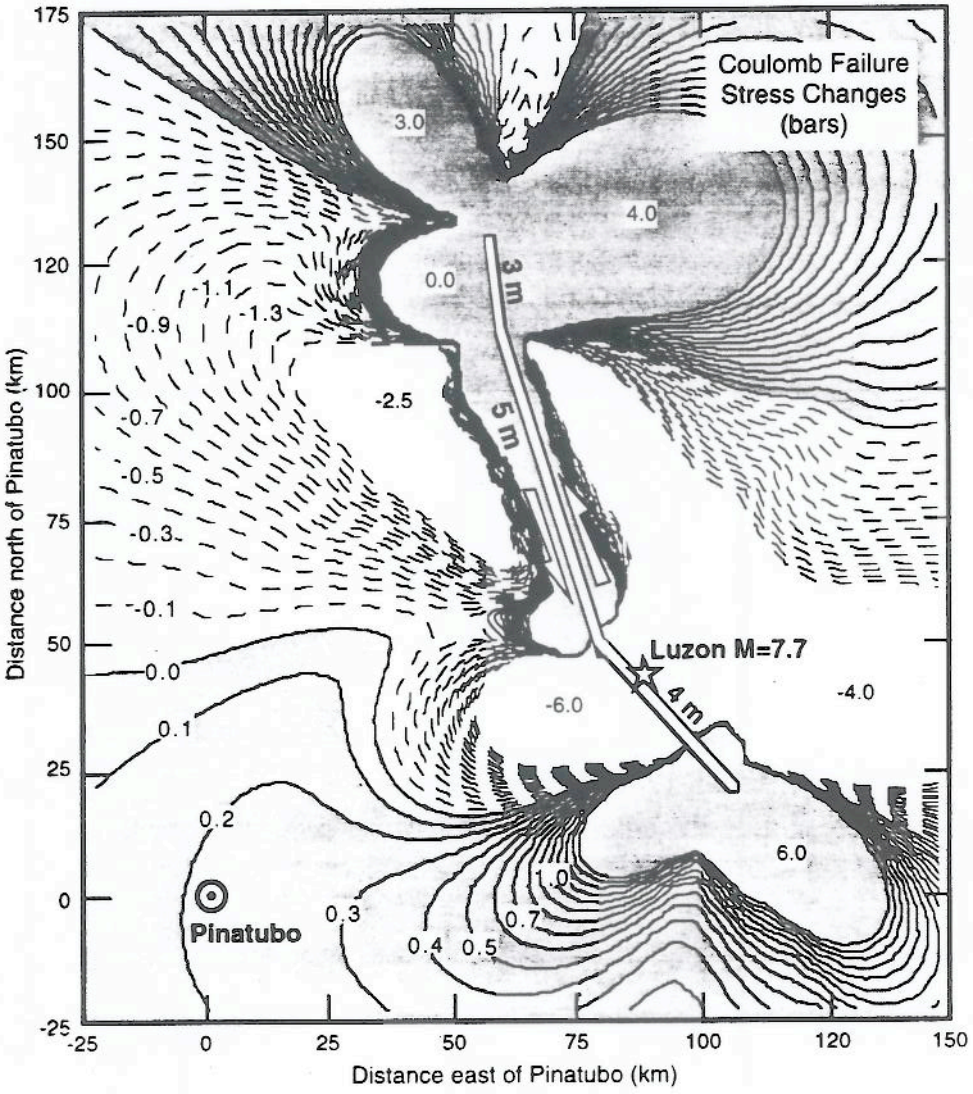

Figure 14. Coulomb stress change on optimally oriented strike-slip or thrust faults to 10 km in depth. Assumptions: Luzon earthquake left-lateral strike-slip on a 20-km-deep vertical fault; east-west compressive regional stress of 100 bar; coefficient of friction=0.4. Small, 0.1- to 0.2-bar increase in Coulomb stress at Pinatubo.

Harlow, this volume) would have been conducive to such a mechanism. The second case would be more consistent with inferences that the Pinatubo eruption was triggered by intrusion of basaltic magma from depth into the base of the dacitic reservoir (Pallister and others, this volume; White and others, this volume).

Alternatively, strong ground shaking during the July 16 earthquake itself might have squeezed a small amount of basaltic magma into the dacitic reservoir or caused pore-pressure changes and thus fault movement that allowed magma ascent. In either of these mechanisms, relatively small and transient effects from the Luzon earthquake itself would have triggered a cascading series of other changes that ultimately led to more basaltic intrusion into the dacitic reservoir, and the full eruption.

Because stress changes caused by the Luzon earthquake are small in relation to a typical, 100-bar compressive stress associated with subduction, that earthquake caused little change in the orientation of stress in the Pinatubo area. If we assume 100-bar east-west compression before the Luzon earthquake, stress after that earthquake is changed only very slightly, to 100.41 bar with a 2.4° counterclockwise rotation. Most focal mechanisms are so controlled by preexisting faults that we would not expect mechanisms to change even with stronger and azimuthally distinct stress changes (J. Mori, USGS, written commun., 1994), and certainly we have no evidence from focal mechanisms determined in 1991 and 1992 of any change from the inferred pre-1990 stress field.

CONCLUSIONS

Occurrence of several earthquakes in the Pinatubo region within days of the main July 16, 1990, Luzon earthquake suggests a possible causal relation between Pinatubo

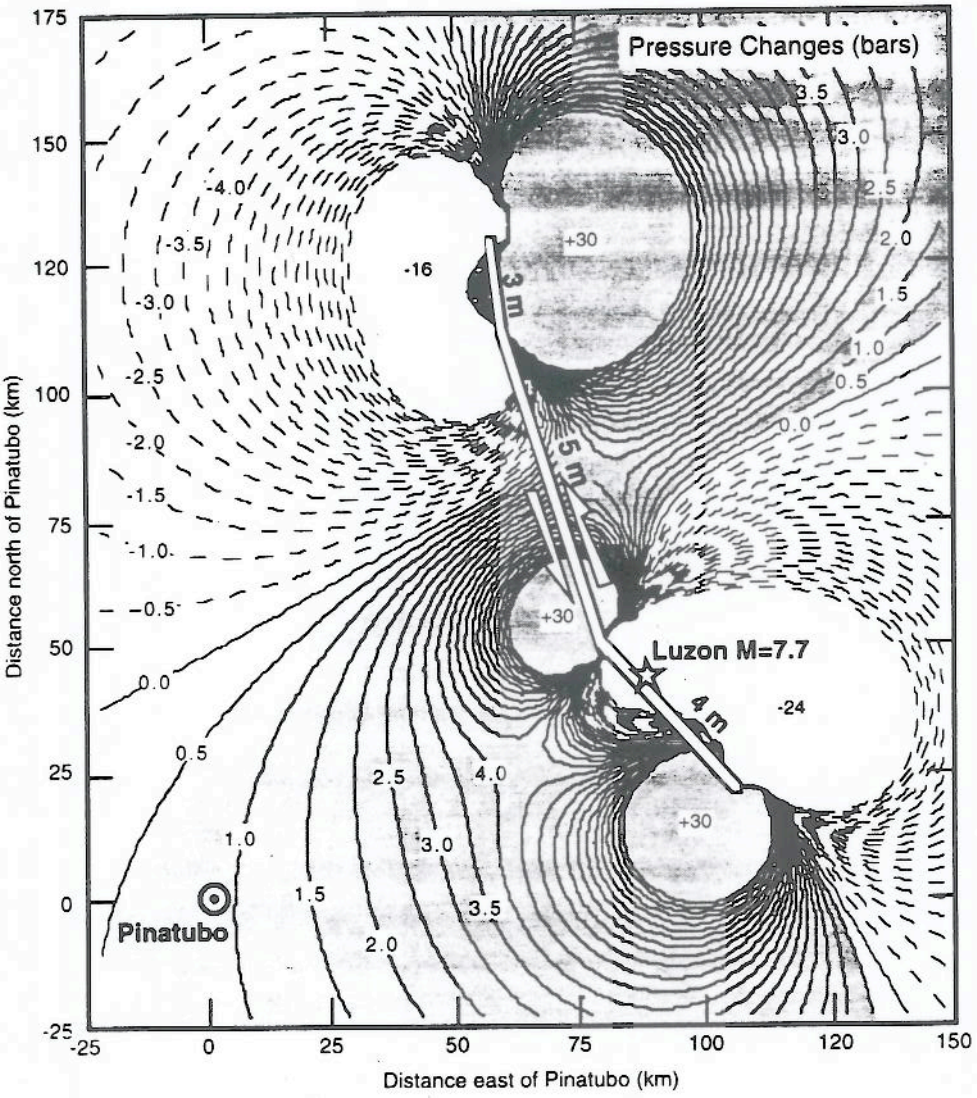

Figure 15. Volumetric stress (pressure) changes at 10 km depth caused by the Luzon earthquake. Assumptions: Luzon seismic moment (M_o) = 3.5×10^{27} dyne-cm (moment magnitude = 7.7); event approximated by left-lateral strike-slip on a 20-km-deep vertical fault. Volumetric stress increase of about 1 bar at Pinatubo.

events and the mainshock. However, Pinatubo is outside the zone of most aftershocks.

The first earthquakes of the 1991 volcanic unrest, defining a northwest cluster, were caused by left-lateral movement along the northwest-trending Maraunot fault, consistent with preexisting, regional east-west compression. The preeruption steaming vents and fissure may have been along a conjugate, northeast-trending fault, also consistent with east-west compression. In contrast, the composite plot of the preeruption summit earthquakes showed highly mixed polarities for each station, suggesting diverse mechanisms that are characteristic of earthquakes caused by magmatic intrusion. Crustal readjustments continued during the posteruption stage, as reflected by several clusters of hypocenters with a wide range of depths and distances from the volcanic center. Such readjustment occurred on structures consistent with regional east-west compressional stress.

Several moderately large syneruption strike-slip earthquakes apparently occurred along preexisting regional faults, in response to volume changes in the magma chamber during the eruption. None of these showed a pure gravity mechanism. Thus, from seismic evidence, the 1991 Pinatubo caldera formed (1) too slowly to generate earthquakes or (2) by the collapse of many small pieces with associated small-magnitude earthquakes.

Changes in Coulomb failure stress as a result of the July 16, 1990, earthquake were small (at most, 10 times larger than tidal stress); compressive stress on the magma reservoir itself was about 1 bar, possibly enough to squeeze basaltic magma into the dacitic reservoir or dacitic magma upward from that reservoir. Alternatively, strong ground shaking during the July 16 earthquake triggered all that followed.

While this study was able to answer some of the Pinatubo puzzles by use of seismic methods, it also opened

up a number of difficult questions that we cannot yet address. Some of these questions are:

- What triggered shallow (5-km-deep) seismicity along the Maraunot fault during April and May 1991? Did regional stress trigger magma ascent, or did magma ascent or inflation of a deep magma reservoir trigger movement along a previously stressed fault?
- Why was the northeast-trending fracture that formed on April 2, 1991, seismically inactive during the period of preeruption seismic monitoring (April 5 through June 12)?
- If 1990 movement along the Philippine fault did not induce a strong stress field in the Pinatubo area, what caused aftershocks in that area immediately after the earthquakes (table 1)? Were the structures along which aftershocks occurred already highly stressed prior to the July 16 Luzon earthquake, allowing strong ground motion from the July 16 earthquake to trigger secondary movements?
- Lastly, do past movements along nearby segments of the Philippine fault (as yet, mostly undated) correlate with dates of past eruptions? Slip along the Philippine fault in A.D. 1645 (Hirano and others, 1986) does not seem to correlate with the penultimate Buag eruptions of Pinatubo (600 to 500 yr B.P.; Newhall and others, this volume). Alternatively, do earthquakes associated with the Manila trench correlate with past eruptions (Javelosa, 1994)? Regrettably, data on prehistoric earthquakes of this region, from the Philippine fault, Manila trench, and other sources are, as yet, too sparse for us to check this correlation.

ACKNOWLEDGMENTS

We would like to acknowledge the help of R.A. White, J. Mori, C.G. Newhall, and an anonymous reviewer for encouragement and for painful but constructive suggestions. We give special thanks to Russ Needham, USGS/NEIC, for determining fault plane mechanisms of syneruption earthquakes, B.J.T. Punongbayan for the initial drafts of the figures and to T. Ohkura, E.G. Ramos, and R.A. White for helping us to produce the revised figures.

REFERENCES CITED

Bautista, B.C., Bautista, M.L.P., Rasdas, A.R., Lanuza, A.G., Amin, E.Q., and Delos Reyes, P.J., 1992, The 16 July 1990 earthquake and its aftershock activity, *in* The July 16, 1990 Luzon Earthquake: A Technical Monograph: Manila, Department of Environment and Natural Resources and the Interagency Committee for Documenting and Establishing Database of the July 1990 Earthquake, p. 81–118.

Bautista, B.C., and Narag, I.C., 1992, FOCPLOT—Computer Program for Plotting Composite Focal Mechanisms: unpublished computer program, Quezon City, PHIVOLCS.

de Boer, J.Z., Odom, L.A., Ragland, P.C., Snider, F.G., and Tilford, N.R., 1980, The Bataan orogene: Eastward subduction, tectonic rotations, and volcanism in the western Pacific (Philippines): Tectonophysics, v. 67, p. 305–317.

Delfin, F.G., Jr., 1984, Geology of the Mt. Pinatubo Area: unpublished report, Manila, Philippine National Oil Company, 36 p.

Delfin, F.G., Jr., Villarosa, H.G., Layugan, D.B., Clemente, V.C., Candelaria, M.R., Ruaya, J.R., this volume, Geothermal exploration of the pre-1991 Mount Pinatubo hydrothermal system.

Ewert, J.W., Lockhart, A.B., Marcial, S., and Ambubuyog, G., this volume, Ground deformation prior to the 1991 eruptions of Mount Pinatubo.

Filson, J., Simkin, T., and Leu, L-K., 1973, Seismicity of a caldera collapse: Galapagos Islands 1968: Journal of Geophysical Research, v. 78, p. 8591–8622.

Harlow, D.H., Power, J.A., Laguerta, E.P., Ambubuyog, G., White, R.A., and Hoblitt, R.P., this volume, Precursory seismicity and forecasting of the June 15, 1991, eruption of Mount Pinatubo.

Hill, D.P., Reasenberg, P.A., Michael, A., Arabaz, W.J., Beroza, G., Brumbauch, D., Brune, J.N., Castro, R., Davis, S., dePolo, D., Ellsworth, W.L., Gomberg, J., Harmsen, S., House, L., Jackson, S.M., Johnston, M.J.S., Jones, L., Keller, R., Malone, S., Munguia, L., Nava, S., Pechmann, J.C., Sanford, A., Simpson, R.W., Smith, R.B., Start, M., Stickney, M., Vidal, A., Walter, S., Wong, V., and Zollweg, J., 1993, Seismicity remotely triggered by the M 7.3 Landers, California earthquake: Science, v. 260, p. 1617–1623.

Hirano, S., Nakata, T., and Sangawa, A., 1986, Fault topography and Quaternary faulting along the Philippine fault zone, central Luzon, Philippines: Journal of Geography [Japan], v. 95, p. 71–93.

Hirn, A., Lepine, J-C., Sapin, M., and Delorme, H., 1991, Episodes of pit-crater collapse documented by seismology at Piton de la Fournaise: Journal of Volcanology and Geothermal Research, v. 47, p. 89–104.

Hoblitt, R.P., Wolfe, E.W., Scott, W.E., Couchman, M.R., Pallister, J.S., and Javier, D., this volume, The preclimactic eruptions of Mount Pinatubo, June 1991.

Javelosa, R.S., 1994, Active Quaternary environments in the Philippine mobile belt: unpublished Ph.D. thesis, Enschede, The Netherlands, International Institute for Aerospace Survey and Earth Sciences (ITC), 179 p.

Lee, W.H.K., ed., 1989, Toolbox for seismic data acquisition, processing, and analysis: IASPEI Software Library, v. 1, Seismological Society of America.

Lee, W.H.K., and Lahr, J.C., 1975, HYPO71 (revised): A computer program for determining hypocenter, magnitude, and first motion pattern of local earthquakes: U.S. Geological Survey Open-File Report 75–311, p. 1–116.

Lockhart, A.B., Marcial, S., Ambubuyog, G., Laguerta, E.P., and Power, J.A., this volume, Installation, operation, and technical specifications of the first Mount Pinatubo telemetered seismic network.

McKee, C.O., Lowenstein, P.L., De Saint Ours, P., Talai, B., Itikarai, I., and Mori, J., 1984, Seismic and ground deformation

crises at Rabaul Caldera: Prelude to an eruption?: Bulletin of Volcanology, v. 47, no. 2, p. 397–411.

Mori, J., Eberhart-Phillips, D., and Harlow, D.H., this volume, Three-dimensional velocity structure at Mount Pinatubo, Philippines: Resolving magma bodies and earthquakes hypocenters.

Mori, J., and McKee, C., 1986, Outward-dipping ring-fault structure at Rabaul caldera as shown by earthquake locations: Science, v. 235, p. 193–195.

Mori, J., White, R.A., Harlow, D.H., Okubo, P., Power, J.A., Hoblitt, R.P., Laguerta, E.P., Lanuza, L., and Bautista, B.C., this volume, Volcanic earthquakes following the 1991 climactic eruption of Mount Pinatubo, Philippines: Strong seismicity during a waning eruption.

Murray, T.L., Power, J.A., March, G.D., and Marso, J.N., this volume, A PC-based realtime volcano-monitoring data-acquisition and analysis system.

Nakamura, K., 1971, Volcano as a possible indicator of crustal strain: Bulletin of the Volcanological Society of Japan, v. 16, p. 63–71. (In Japanese with English abstract.)

Newhall, C.G., Daag, A.S., Delfin, F.G., Jr., Hoblitt, R.P., McGeehin, J., Pallister, J.S., Regalado, M.T.M., Rubin, M., Tamayo, R.A., Jr., Tubianosa, B., and Umbal, J.V., this volume, Eruptive history of Mount Pinatubo.

Newhall, C.G., and Dzurisin, D., 1988, Historical unrest at large calderas of the world: U.S. Geological Survey Bulletin 1855, 1,108 p.

Pallister, J.S., Hoblitt, R.P., Meeker, G.P., Knight, R.J., and Siems, D.F., this volume, Magma mixing at Mount Pinatubo: Petrographic and chemical evidence from the 1991 deposits.

Power, J.A., Murray, T.L., Marso, J.N., and Laguerta, E.P., this volume, Preliminary observations of seismicity at Mount Pinatubo by use of the Seismic Spectral Amplitude Measurement (SSAM) system, May 13–June 18, 1991.

Ramos, A.F., and Isada, M. G., 1990, Emergency investigation of the alleged volcanic activity of Mount Pinatubo in Zambales Province: PHIVOLCS, Memorandum Report, 2 p.

Ramos, E.G., Laguerta, E.P., and Hamburger, M.W., this volume, Seismicity and magmatic resurgence at Mount Pinatubo in 1992.

Rikitake, T., and Sato, R., 1989, Up-squeezing of magma under tectonic stress: Journal of Physics of the Earth, v. 37, p. 303–311.

Rivera, L., and Cisternas, A., 1990, Stress tensor and fault plane solutions for a population of earthquakes: Bulletin of the Seismological Society of America, v. 80, no. 3, p. 600–614.

Sabit, J.P., Pigtain, R.C., and de la Cruz, E.G., this volume, The west-side story: Observations of the 1991 Mount Pinatubo eruptions from the west.

Scott, W.E., Hoblitt, R.P., Torres, R.C., Self, S, Martinez, M.L., and Nillos, T., Jr., this volume, Pyroclastic flows of the June 15, 1991, climactic eruption of Mount Pinatubo.

Stein, R.S., King, G.C.P., and Lin, J., 1992, Change in failure stress on the southern San Andreas fault system caused by the 1992 magnitude=7.4 Landers earthquake: Science, v. 258, p. 1328–1332.

Valdes, C., 1989, PCEQ, A computer program for picking earthquake phases, *in* IASPEI software library: Seismological software for IBM-compatible computers: International Association of Seismology and Physics of the Earth's Interior, and Seismological Society of America.

White, R.A., this volume, Precursory deep long-period earthquakes at Mount Pinatubo, Philippines: Spatio-temporal link to a basalt trigger.

Xu, Z., Wang, S., Huang, Y., and Gao, A., 1992, Tectonic stress field of China inferred from a large number of small earthquakes: Journal of Geophysical Research, v. 97, no. B8, p. 11867–11877.

Zoback, M.D., and Zoback, M.L., 1991, Tectonic stress field of North America and relative plate motions, *in* Slemmons, D.B., Engdahl, E.R., Zoback, M.D., and Blackwell, D.D., eds., Neotectonics of North America: Boulder, Geological Society of America, Decade Map Volume 1, p. 339–366.

Zoback, M.L., 1992, First- and second-order patterns of stress in the lithosphere; the world stress map project: Journal of Geophysical Research, v. 97, no. B8, p. 11703–11728.